Astronomy & Astrophysics manuscript no. as-pks
December 18, 2014
© ESO 2014

arXiv:1412.5408v1 [astro-ph.GA] 17 Dec 2014

The inhomogeneous ISM toward PKS 1830–211 SW - A detailed view on molecular gas at a look-back time of 7.5 Gyr

A. Schulz[1,2], C. Henkel[3,4], K. M. Menten[3], S. Muller[5], D. Muders[3], J. Bagdonaite[6], and W. Ubachs[6]

[1] Argelander-Institut für Astronomie, Universität Bonn, Auf dem Hügel 71, 53121 Bonn, Germany
[2] Institut für Physik und ihre Didaktik, Universität zu Köln,, Gronewaldstr. 2, 50931 Köln, Germany
[3] Max-Planck-Institut für Radioastronomie, Auf dem Hügel 69, D-53121 Bonn, Germany
[4] Astron. Dept., King Abdulaziz University, P.O. Box 80203, Jeddah 21589, Saudi Arabia
[5] Dept. of Earth and Space Sciences, Chalmers University, Onsala Space Observatory, 43992 Onsala, Sweden
[6] Dept. of Physics and Astronomy, VU University Amsterdam, De Boelelaan 1081, 1081 HV Amsterdam, Netherlands

Received: date / Accepted: (n)ever

ABSTRACT

Based on measurements with the Effelsberg 100-m telescope, a multi-line study of molecular species is presented toward the south-western source of the gravitational lens system PKS 1830–211, which is by far the best known target to study molecular gas in absorption at intermediate redshift. Determining line parameters and optical depths and performing Large Velocity Gradient radiative transfer calculations, the aims of this study are (1) to evaluate physical parameters of the absorbing foreground gas at $z \sim 0.89$, in particular its homogeneity, and (2) to monitor the spectroscopic time variability caused by fluctuations of the $z \sim 2.5$ background continuum source. We find, that the gas is quite inhomogeneous with $n(\mathrm{H_2}) \sim 2 \times 10^3\,\mathrm{cm^{-3}}$ for most molecular species but with higher values for $\mathrm{H_2CO}$ and lower ones for SO. Measuring the CS J=1←0 transition during a time interval of more than a decade, from 2001 to 2012, the peak absorption depth of the line remains approximately constant, while the line shape undergoes notable variations. Covering the time between 1996 and 2013, CS, $\mathrm{HCO^+}$, and $\mathrm{CH_3OH}$ data indicate maximal integrated optical depths in ∼2001 and 2011/2012. This is compatible with a ∼10 yr periodicity, which, however, needs confirmation by substantially longer time monitoring. Comparing molecular abundances with those of different types of Galactic and nearby extragalactic clouds we find that the observed cloud complex does not correspond to one particular type but to a variety of cloud types with more diffuse and denser components as can be expected for an observed region with a transverse linear scale of several parsec and a likely larger depth along the line-of-sight. A tentative detection of Galactic absorption in the c-$\mathrm{C_3H_2}$ $1_{10} - 1_{01}$ line at 18.343 GHz is also reported.

Key words. Galaxies: abundances – Galaxies: ISM – Galaxies: individual: PKS 1830–211 – Gravitational lensing – Radio lines: galaxies

1. Introduction

To study molecular cloud properties in far distant galaxies, low spatial resolution becomes an increasingly important problem since every observed position is averaging over large areas. Furthermore beam filling factors are small causing low flux densities and, therefore, low signal-to-noise ratios. A suitable way to overcome these problems is to use molecular lines in absorption in front of compact background continuum sources such as radio quasars whose small angular sizes determine the effective beam size of the observation and whose continuum flux densities determine the sensitivity of the measurements. The availability of such background-foreground pairs and the required strength of the background continuum limit the application of this method to a very small number of objects. The so far brightest and most distant such pair is PKS 1830–211 (Wiklind & Combes 1996a), a gravitational lens with truly unique properties. The background source is likely a blazar at $z = 2.507$ (Lidman et al. 1999, De Rosa et al. 2005). The foreground lens is a spiral galaxy observed almost face-on at redshift $z \sim 0.89$ (Courbin et al. 2002; Winn et al. 2002). It splits the continuum radiation of the blazar into three main image components. These consist of a stronger north-eastern "hotspot", a weaker south-western "hotspot", and an Einstein ring being prominent only at low frequencies (<10 GHz; Jauncey et al. 1991). The SW source is located behind a spiral arm of the lensing galaxy, at a distance of about 2 kpc from its center (Muller et al. 2006), and shows by far the strongest molecular absorption lines among all known sources of its class (for the others, see Wiklind & Combes 1994, 1995, 1996b and Kanekar et al. 2005).

The exceptional situation concerning continuum flux and line strength encountered in PKS 1830–211 has been extensively explored, leading to a large number of detected molecular lines and species (e.g., Henkel et al. 2009; Muller et al. 2011, 2014a,b). Therefore it provides detailed insight into the properties of the interstellar medium of a galaxy at an intermediate cosmological distance. Adopting a standard Λ-cosmology with $\mathrm{H_0} = 67\,\mathrm{km\,s^{-1}\,Mpc^{-1}}$, $\Omega_\mathrm{m} = 0.315$, and $\Omega_\Lambda = 0.685$ (Planck Collaboration et al. 2014), $z = 0.88582$ corresponds to a lookback time of about 7.5 Gyr, more than half the present age of the universe.

Send offprint requests to: A. Schulz, e-mail: andreas.schulz@uni-koeln.de

It is the aim of this article to examine physical properties of the molecular gas using molecular lines characterizing various physical conditions. This includes a first evaluation of the homogeneity of the absorbing molecular gas column and CS $J = 1 \leftarrow 0$ spectra covering more than a decade to study variability caused by the background continuum source.

2. Observations

The observations were carried out in a position switching mode with the primary focus $\lambda = 1.9$, 1.3, and 1.0 cm receivers of the 100-m telescope at Effelsberg/Germany[1], mostly within the short period between August and December 2001. On- and off-source integration times were two minutes per scan, yielding full cycles of 4–5 minutes duration. For full width to half power (FWHP) beam widths, system temperatures, and aperture efficiencies, see Table 1. During 2001–2006, the backend was an 8192 channel autocorrelator, which was split into eight segments, covering selected frequency ranges within a total bandwidth of 500 MHz. Each of the eight segments had a bandwidth of 40 MHz with 512 channels, yielding channel spacings of 0.7–1.7 km s^{-1}. At $\lambda \sim 1.3$ cm, but not at 1.9 and 1.0 cm, a dual channel receiver was used sampling orthogonal linear polarizations. Therefore, in this case at least two of the eight segments were centered at the same frequency to maximize sensitivity by observing simultaneously the two polarization components. In 2006, a Fast Fourier Transform Spectrometer (FFTS) was employed with a bandwidth of 100 MHz and 16384 channels for each polarization channel. For the more recent CS data from April 2011 to April 2012 another FFTS was used, this time with a bandwidth of 2 GHz and 32768 channels per polarization. At 26 GHz, the corresponding FFTS channel spacings are 0.07 and 0.7 km s^{-1}, respectively. For recent (2012/3) methanol measurements, the 32768 channel FFTS has also been used, but in this case with a bandwidth of 100 MHz. Details of these recent methanol observations can be found in Bagdonaite et al. (2013a,b).

As already mentioned (Sect. 1), PKS 1830–211 is with $\sim$5 Jy near $\lambda = 1$ cm one of the strongest continuum sources in the radio sky. Therefore, focus and pointing could be checked toward the source itself. The latter was found to be accurate to about 5″. The continuum was also used to calibrate the spectral lines to obtain line-to-continuum flux density ratios, which could be determined with an accuracy of up to ±7% depending on the strength of the respective line (see also Sect. 4). Data reduction was obtained using standard procedures of CLASS and GREG, two tools of the GILDAS[2] software package. During the data reduction, only linear baselines were subtracted from the original spectra.

3. Results

The separation between the north-eastern and south-western hotspots of PKS 1830–211 (see Sect. 1) is about 1 arcsec. Therefore, they are clearly within our much larger beam sizes (Table 1). Figure 1 shows the line profiles measured at Effelsberg between August and December 2001, with the ordinate displaying absorption in units of percent of the total observed continuum flux density. The abscissa depicts Local Standard of Rest (LSR) velocity relative to $z = 0.88582$. The detected absorption lines originate all from the SW hotspot. We have obtained five spectra (one containing two lines) of the molecules SO, para-c-C_3H_2, CH_3OH, and ortho-H_2CO. While, in the meantime, these molecules have also been detected in other studies (e.g., Muller et al. 2011), these are the earliest detections except for H_2CO and C_3H_2 (Menten et al. 1999). The spectra do not show absorption line components at an LSR velocity of about –135 km s^{-1}, which might appear in front of the NE hotspot (Wiklind & Combes 1998, Muller et al. 2006). Fig. 2 depicts our tentative detection of Galactic C_3H_2, which would be the first detection of Galactic molecular gas absorption toward the line-of-sight to PKS 1830–211.

Table 1. Observational parameters.

ν (GHz)	λ (cm)	$\theta_b^{a)}$ (″)	$T_{sys}^{b)}$ (K)	$\eta_A^{c)}$
13.5–18.7	1.9	60–45	40	0.39–0.32
18.0–26.0	1.3	45–35	70	0.33–0.26
27.0–36.7	1.0	32–23	75	∼0.30

a) Full Width to Half Power (FWHP) beam width in arcsec.
b) System temperatures in units of antenna temperature (T_A^*).
c) Aperture efficiency.

Apparent optical depths are determined using

$$\tau_{app} = -\ln\left(1 - \frac{|T_L|}{T_C}\right)$$

(e.g., Henkel et al. 2009), with T_L and T_C denoting line and continuum temperature and assuming (realistically) that the excitation temperature T_{ex} is negligible relative to T_C (see also Sect. 4.4). Line parameters and apparent optical depths are given in Table 2. The table also contains upper limits to the optical depths of six molecular transitions and two recombination lines, also obtained between August and December 2001, and additional data taken from the literature. The noise level of the data with detected absorption does not allow us to discriminate between several velocity components as it has been done, for example, by Henkel et al. (2009) when analyzing their CS J=1←0 profile.

Within the limits of noise, all the main line components obtained in 2001 show similar velocities (see also Henkel et al. 2008 and 2009 for additional lines at $\lambda \sim$ 1–2 cm). The Local Standard of Rest (LSR) velocities of the peaks of the absorption (LSR velocities will be used throughout the paper), are close to ∼9–10 km s^{-1}. Fig. 3 displays CS $J = 1 \leftarrow 0$ spectra from the south-western component taken over a time interval of more than a decade, from 2001 to 2012. Table 3 summarizes the corresponding line parameters.

[1] The 100-m telescope at Effelsberg is operated by the Max-Planck-Institut für Radioastronomie (MPIfR) on behalf of the Max-Planck-Gesellschaft (MPG).

[2] Grenoble Image and Line Data Analysis Software, see http://www.iram.fr/IRAMFR/GILDAS

Table 2. Line parameters and derived optical depths

Transition	$\nu_{observed}$ (GHz)	ν_{rest} (GHz)	V (km s^{-1})	ΔV (km s^{-1})	f_c	τ	τ f_c= .38	$\Delta\tau$	Remarks
Our Detections									
H_2CO $3_{12} \leftarrow 3_{13}$(o)	15.36456	28.97480	8.9±2.7	27.1±5.3	.153	.054	.021	30%	070801
SO $1_0 \leftarrow 0_1$	15.90902	30.00154	7.5±0.4	5.4±1.2	.156	.031	.013	10%	140801, 1
			5.8±2.4	37.2±5.8	.156	.016	.006	25%	140801, 1
c − C_3H_2 $1_{10} \leftarrow 1_{01}$(o)	18.34314	18.34314	4.6±0.6	5.1±1.5	1.00	.007	—	$\gtrsim$ 30%	151201, 2
CH_3OH $1_0 \leftarrow 0_0(A^+)$	25.65063	48.37247	8.7±0.5	8.3±1.4	.196	.065	.033	20%	231201, 3
CH_3OH $1_0 \leftarrow 0_0$(E)	25.65297	48.37689	8.7±1.3	5.1±4.9	.196	.020	.010	100%	231201, 3
c − C_3H_2 $1_{11} \leftarrow 0_{00}$(p)	27.49012	51.84141	10.2±0.7	15.4±2.3	.198	.097	.050	20%	290901
SO $2_1 \leftarrow 1_0$	33.37105	62.93179	8.6±1.1	20.9±2.5	.227	.063	.038	20%	011001
Our Nondetections									
HC_5N 13 ← 12	18.35508	34.61439	–	–	.17	<.003	<.001	7%	151201, 4
SiS 2 ← 1	19.25403	36.30963	–	–	.17	<.002	<.001	7%	151201, 4
H56α	19.33709	36.46627	–	–	.17	<.018	<.008	7%	151201, 4
H70β	19.49376	36.76172	–	–	.17	<.018	<.008	7%	151201, 4
HNCO $2_{02} \leftarrow 1_{01}$	23.31249	43.96300	–	–	.19	<.004	<.002	7%	301201, 4
HC_5N 20 ← 19	28.23830	53.25235	–	–	.21	<.005	<.003	7%	031001, 4
SO_2 $2_{11} \leftarrow 2_{02}$	28.38493	53.52887	–	–	.22	<.006	<.004	7%	031001, 4
SO $3_4 \leftarrow 3_3$	35.01657	66.03494	–	–	.23	<.009	<.006	7%	021001, 4
Menten et al. (1999)									
H_2CO $2_{11} \leftarrow 2_{12}$(o)	07.68285	14.48848	∼9	∼20	.20	.050	.026	15%	5
c − C_3H_2 $2_{12} \leftarrow 1_{01}$ (o)	45.25294	85.33891	∼9	∼20	.35	.210	.190	15%	5, 7
Muller et al. (2011)									
c − C_3H_2 $3_{31} \leftarrow 3_{22}$(p)	31.58196	59.55789	–	–	.22	.005	.003	20%	6
CH_3OH $1_0 \leftarrow 2_{-1}$ (E)	32.09821	60.53146	7.1±0.5	21.2±1.2	.22	.033	.019	10%	6
SO $2_1 \leftarrow 1_0$	33.37105	62.93180	11.4±0.3	19.7±0.7	.23	.050	.030	10%	6
c − C_3H_2 $2_{02} \leftarrow 1_{11}$(p)	43.53202	82.09356	–	–	.26	.084	.057	10%	6
c − C_3H_2 $3_{12} \leftarrow 3_{03}$(o)	43.99476	82.96621	11.5±0.1	18.7±0.2	.26	.031	.022	10%	6
c − C_3H_2 $2_{12} \leftarrow 1_{01}$(o)	45.25294	85.33891	–	–	.26	.285	.189	10%	6, 7
SO $2_2 \leftarrow 1_1$	45.65332	86.09395	–	–	.27	.004	.003	35%	6

"Our Detections" and "Our Nondetections" were all obtained between August and December 2001.
Col. (1): Molecular line, (o)=ortho, (p)=para; Col. (2): redshifted frequency, adopting $z = 0.88582$; Col. 3: Approximate rest frequency; Cols. (4) and (5): Local Standard of Rest velocities and full width to half power (FWHP) line widths, in case of SO $1_0 \leftarrow 0_1$ for both the broad and the narrow component; Cols. (6) and (7): continuum source covering factor (see also Sect. 4.1 and Henkel et al. 2009) and corresponding peak optical depth(s); Col. (8): peak optical depths for a continuum source covering factor of 0.38; Col. (9): estimated 1σ uncertainties in percent of the optical depth.
Remarks (last column):
The 6-digit numbers provide the epoch of our observations with day, month, and year from left to right.
1: Possibly two line components.
2: Galactic line, tentative detection. A continuum source covering factor of unity has been adopted.
3: E- and A-transitions seen in the same spectrum (Fig.1). The intensities are consistent with a line strength ratio of 1:3.8.
4: Upper 1σ limits of τ; spectra were smoothed to ∼10 km s^{-1} channels.
5: Extrapolated continuum flux densities: 7.1 Jy (14 GHz) and 3.5 Jy (45 GHz).
6: Calculated from Table 10 of Muller et al. (2011).
7: τ values of Menten et al. (1999) and Muller et al. (2011) agree well.

4. Analysis

4.1. Source covering factor and time variability

In order to determine the true optical depths of our spectra from the south-western source, an important problem to be discussed is the background source coverage factor f_c. Muller et al. (2006) find their HCO^+ feature at 94 GHz being saturated at a depth of 38% relative to the total continuum level implying $f_c = 0.38$ at this frequency (see also Martí-Vidal et al. 2013 and Muller et al. 2014b). Trying to account for a larger extent of the background continuum at lower frequencies, Henkel et al. (2009) proposed a frequency dependence of this factor, $f_c = 0.2 \times(\nu_{\rm observed}/26\,{\rm GHz})^{0.5}$ for $\nu_{\rm observed} \lesssim 100$ GHz, matching that determined by Muller et al. (2006) at the high frequency end. Therefore, we present calculated $\tau_{\rm peak}$ values using both, the constant coverage factor of 0.38 and the frequency-dependent factor in our Table 2. Nevertheless, this affects our analysis only marginally since below we will use ratios of optical depths which lead to results that are

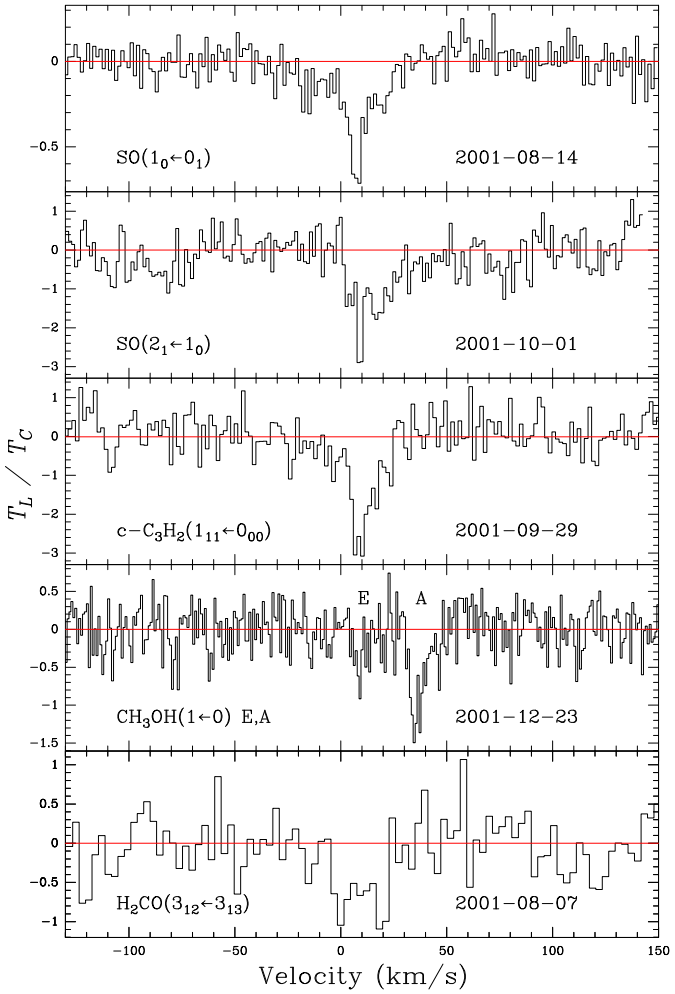

Fig. 1. The six absorption lines detected toward PKS 1830–211, displayed in five panels with a Local Standard of Rest (LSR) velocity scale relative to z=0.88582 ($V_{\rm LSR}$ = $V_{\rm HEL}$ + 12.4 km s^{-1}; ordinate: absorption depth in units of percent of the observed continuum flux density, T_C, accounting for the entire source). The spectra were taken between August and December 2001. The velocity scale of the fourth panel from the top is based on the E-transition of methanol (CH_3OH). The scale for the A-transition is offset by –27.5 km s^{-1}. The cyclic-C_3H_2 line of the central panel belongs to the para species (see Table 2). Channel spacings are 1.4, 1.4, 1.7, 0.9 and 3.0 km s^{-1} from top to bottom.

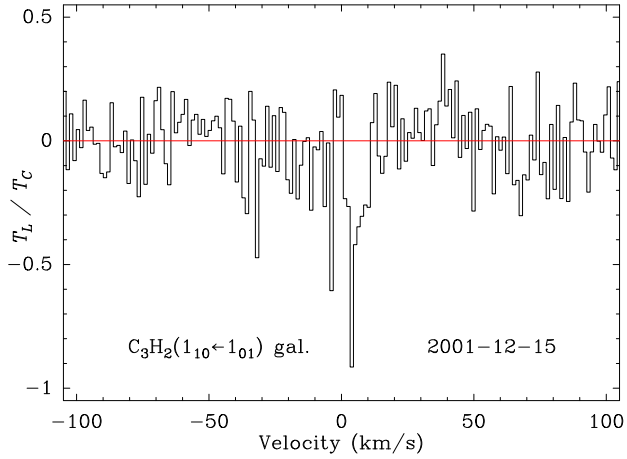

Fig. 2. The tentative detection of Galactic c-C_3H_2 (cyclic variant, ortho-species), with a channel spacing of 1.3 km s^{-1}. The spectrum was taken on December 15, 2001. The ordinate denotes absorption in units of percent of the entire observed continuum flux density, T_C, of PKS 1830–211. The abscissa is Local Standard of Rest velocity for redshift zero.

Table 3. CS J = 1←0 one component Gaussian fit parameters[a])

Epoch	$\int (T_{\rm L}/T_{\rm c}){\rm d}V$	$V_{\rm LSR}$ (km s^{-1})	ΔV
Dec. 15, 2001	–4.43±0.07	10.6±0.2	23.5±0.5
Dec. 22, 2001	–4.42±0.11	09.8±0.3	24.9±0.8
Dec. 30, 2001	–4.38±0.05	11.3±0.1	22.1±0.3
Mar. 11, 2002	–4.76±0.05	09.6±0.1	26.4±0.3
Sep. 27, 2002	–4.42±0.06	11.0±0.1	23.4±0.4
Jan. 05, 2003	–3.57±0.04	11.5±0.1	19.1±0.2
Mar. 18, 2006	–3.13±0.04	10.9±0.1	15.5±0.2
Apr. 01. 2011	–3.32±0.04	09.9±0.1	18.3±0.3
Dec. 08, 2011	–4.28±0.03	10.3±0.1	19.4±0.1
Apr. 08, 2012	–4.60±0.02	10.1±0.1	20.0±0.1

[a]) Adopted redshifted frequency: ν = 25.978596 GHz. Note that the absorption peak is slightly (typically 1.0–2.5 km s^{-1}) blue-shifted with respect to the velocities given in Col. 3, caused by the asymmetry in the overall lines (Fig. 3). For integrated optical depths, see Fig. 4.

quite independent of coupling values because frequencies are not too discrepant.

Another problem discussed in the literature are concerns about the variability of the source (e.g., Muller & Guélin 2008). Henkel et al. (2009) find that the depth of the absorption features is well correlated with the continuum flux. Since all our observations presented here for the first time with the notable exception of CS J = 1←0 were carried out during a short period within 2001 (see also Sect. 2 and Table 2), being confined to epochs within the observing period covered by Henkel et al. (2009), variations in the ratio of line intensity to continuum flux remain negligible.

A further important point is whether this argumentation also holds when using data taken over a longer time span. This seems to be the case because two lines relevant for this study were observed at two largely different epochs: (1) The ortho c-C_3H_2 2_{12}←1_{01} transition, reported by Muller et al. (2011), was also observed by Menten et al. (1999). The agreement in peak optical depths is excellent (see Table 2). (2) The SO 2_1←1_0 line observed by us in 2001 was also observed by Muller et al. (2011), yielding again, within the error limits, consistent results. We have to note, however, that this agreement may be fortuitous and would not necessarily hold, if we would compare data from other epochs.

To better illustrate this effect, Fig. 3 shows a series of CS (1 ← 0) lines measured between Dec. 2001 and Apr. 2012. The depth of the absorption remains constant to within the calibration uncertainties (see Sect. 2), while the line shape is slowly varying. The component at about –10 km s^{-1} fades in 2002. The one at about +18 km s^{-1} disappears between 2006 and 2011. In spring 2012, the pro-

file becomes almost Gaussian, suggesting that the velocity range with a significant optical depth (larger than unity) has increased. Comparing these data with the observations by Muller et al. (2008) of the even more saturated HCO^+ J = 2←1 line (their data are presented on a heliocentric velocity scale) also shows a roughly constant absorption depth (implying that f_c remains approximately constant in time, see also Muller et al. 2006, Henkel et al. 2009), the fading of the –10 km s^{-1} component, and a trend to a more Gaussian profile near the end of their monitoring period (May 2007).

To visualize the changes, Fig. 4 displays the integrated optical depths of two main molecular tracers, HCO^+ J = 2←1 and CS 1←0, the latter amplified by a factor of four, to match the other data. Since HCO^+ shows higher optical depths than CS (see Muller & Guélin 2008; Henkel et al. 2009; Muller et al. 2014b), the blue wings of the HCO^+ profiles have been plotted, which show significant variablity, indicating like CS only moderate saturation. The observed trend in integrated line opacity variations shows excellent agreement. To expand the monitored time interval further, we have also included recently taken methanol (CH_3OH) data from Effelsberg (see also Sect. 2), which have been published by Bagdonaite et al. (2013a,b) and which show a significant decrease in integrated opacities from a peak value reached at the end of 2011 or early 2012. Combining these data, we see peaks in 2000–2002 and 2011–2012 and lower values at other times, when considering the time interval between 1995 and 2013. This suggests a period of variability of order 10 yr. Of course, having obtained data from less than two such full periods, this is speculative. Nevertheless, longer term monitoring might yield periodicities which could be related to activity of the background blazar. Accompanied by systematic measurements revealing the spatial fine structure of the line absorption and background continuum, this could probe the activity at the base of a blazar's jet (see, e.g., Nair et al. 2005), also testing the plasmon ejection model proposed by Martí-Vidal et al. (2013).

We thus agree with Muller et al. (2011) that the line shape experiences gradual changes which result in variations of velocity-integrated optical depths. Peak optical depths appear to be less variable than integrated optical depths, but we note that both the HCO^+ 2←1 line (Muller et al. 2008) and, at the very center, our CS 1←0 line show signs of saturation, while below optically thin transitions will be discussed. Nevertheless, in view of occasionally measured broad features with questionable significance, we prefer to focus in the following on peak line intensities and the corresponding optical depths. The measured absorption is better defined by the depth of the (main) feature than by integrated opacities with sometimes poorly defined line widths. The most recent data of Muller et al. (2013) will not be considered because Muller et al. (2013) reported significant variations with respect to their 2009/10-spectra, in good agreement with our findings from CS 1←0 and CH_3OH (see Figs. 3–5).

4.2. Radiative transfer calculations

Among our observed spectra from 2001, only SO is detected in two different transitions. However, to perform radiative transfer modelling for all of our observations, we need at least two different lines for each molecule. We therefore take line data from two other investigations from which

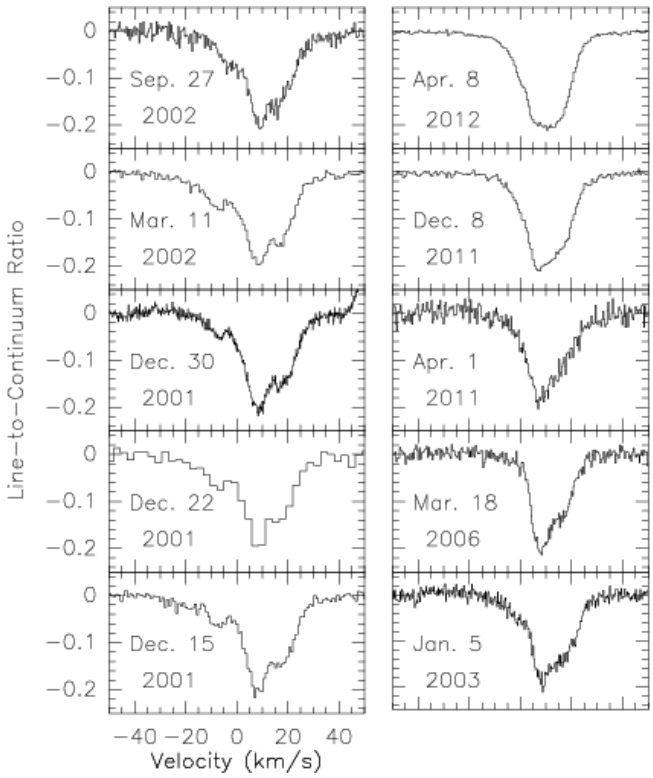

Fig. 3. Monitoring observations of the CS (1←0) line near 26 GHz, covering more than a decade (from lower left to upper right). Channel spacings are (from the earliest to the latest epoch) 0.90, 2.7, 0.22, 0.90, 0.45, 0.34, 0.45, 0.42, 0.70, and 0.70 km s^{-1}. The ordinate denotes absorption in units of the entire continuum flux density of PKS 1830–211. The abscissa is Local Standard of Rest velocity for redshift $z = 0.88582$.

we can derive line center optical depths, from Muller et al. (2011) for HNCO, CH_3OH-E, para and ortho c-C_3H_2 (their Table 10) and Menten et al. (1999) for ortho c-C_3H_2 and H_2CO. As already mentioned in Sect. 4.1 (see also Table 2), these data are compatible, because peak opacities are similar. SO $2_1 \leftarrow 1_0$ opacities from Muller et al. (2011) agree with our data 10 years earlier and the same is the case for c-C_3H_2 $2_{12} \leftarrow 1_{01}$ opacities, when comparing Menten et al. (1999) and Muller et al. (2011).

To reproduce line ratios of the observed molecules, we apply the standard Large Velocity Gradient (LVG) model described by Henkel et al. (2009) assuming a spherically symmetric cloud and constant kinetic temperature and density throughout the emitting region. On one hand, all the molecular lines discussed below absorb less than three percent of the background continuum flux. On the other hand, the continuum source covering factor lies above 0.15 (Muller & Guélin 2008; Henkel et al. 2009; Muller et al. 2014b). Hence, we can be sure (as already suggested in Sect. 4.1) that all the lines are optically thin. This implies that our results do not depend on cloud morphology and, therefore, our assumption of spherical cloud geometry will not affect the results.

In contrast to the work of Muller et al. (2013), we do not assume single values of gas density and temperature common for all molecules in our analysis, which they themselves regard as the major limitation of their excitation analysis.

We have carried out our model calculations for a large variety of densities and temperatures (see Figs. 6–10) examining also those obtained by Henkel et al. (2008, 2009) and Muller et al. (2011).

All data used for the model calculations are contained in Table 2. The basic question is: Are the results consistent with the density and temperature parameters of previous studies, i.e. $T_{\rm kin}$ = 50 or 80 K and $n(H_2)$ = 1000–2000 cm^{-3} (Henkel et al. 2008, 2009; Muller et al. 2011, 2013), the former involving the classical $T_{\rm kin}$ tracers NH_3 and CH_3CN? Because the common degeneracy between high $T_{\rm kin}$/low $n(H_2)$ and vice versa affects most molecular line pairs, including our tracers, there is a wide parameter space for each pair of lines. Here we thus intend to find out whether the above mentioned $T_{\rm kin}/n(H_2)$ combination can reproduce our data in all cases. The results discussed below are valid for both sets of continuum coverage factors (Sect. 4.1 and Table 2), which slightly affect our results only in cases of significantly diverging frequencies of the lines involved.

c – C_3H_2

(p): The observed $2_{02} \leftarrow 1_{11}$ to $1_{11} \leftarrow 0_{00}$ ratio of para-cyclopropenylidene, 0.87±0.19 (f_c = 0.198) or 1.14±0.25 (f_c = 0.38), is – also for the former value within 2σ – compatible with $T_{\rm kin}$ = 50–80 K and $n(H_2)$ = 1000–2000 cm^{-3} (Fig. 6). This agrees with the parameters derived by Henkel et al. (2008, 2009) and Muller et al. (2011, 2013) from multiline studies.

(o): The measured ratio of the ortho $3_{12} \leftarrow 3_{03}$ to $2_{12} \leftarrow 1_{01}$ opacities, 0.110±0.015 (both lines taken from Muller et al. 2011), is well reproduced with the same $T_{\rm kin}$ and $n(H_2)$ (Fig. 7) yielding a column density a few times that of the para-type of the molecule (the precise factor depends on the $T_{\rm kin}$ and $n(H_2)$ parameters chosen), in accordance with the expected factor of three for the ortho/para ratio.

Lines of this molecule commonly originate in moderately dense molecular gas (e.g., Thaddeus et al. 1995; Aladro et al. 2011), and our adopted temperature and density are in accordance with this scenario.

Although the detection of the (Galactic) C_3H_2 ($1_{10} \leftarrow 1_{01}$) feature is tentative, it should not be entirely unexpected since this molecular transition is known to be quite widespread (e.g., Madden et al. 1989) and our source is located not far from the Galactic plane and center ($l^{\rm II}$ = 12.2°, $b^{\rm II}$ = –5.7°). We have checked possible other line identifications in the (Galactic) range of 18.335 to 18.353 GHz as well as in the range 34.581 to 34.600 GHz, redshifted by z = 0.88582, and find no other likely line candidate. There is no previous detection of Galactic molecular absorption lines along this line of sight.

CH_3OH

Quasi-thermal lines of methanol trace warm and at least moderately dense gas ($n(H_2) \gtrsim 1000$ cm^{-3}; e.g., Leurini et al. 2004). The species is easily dissociated, and it is not detected in Galactic clouds of very low density (Liszt et al. 2008). Applying the same kinetic temperature and density as above, the modelled ratio of the opacities of the molecular A and E species becomes 3.8 in case of equal abundances. This agrees within the errors with the observations (Table 2 and Fig. 1) and the more sensitive data from Bagdonaite et al. (2013a,b), taken more than a decade later. Referring to our clearly detected line of the A-species (Fig. 1), dividing its intensity by 3.8, and comparing it with that of the E ($1_0 \leftarrow 2_{-1}$) transition observed by Muller et al. (2011) yields an opacity ratio of 1.8±0.4, which is also consistent with the density estimate by Henkel et al. (2009; see Fig. 8). The kinetic temperature remains poorly constrained and allows for both $T_{\rm kin}$ = 50 and 80 K.

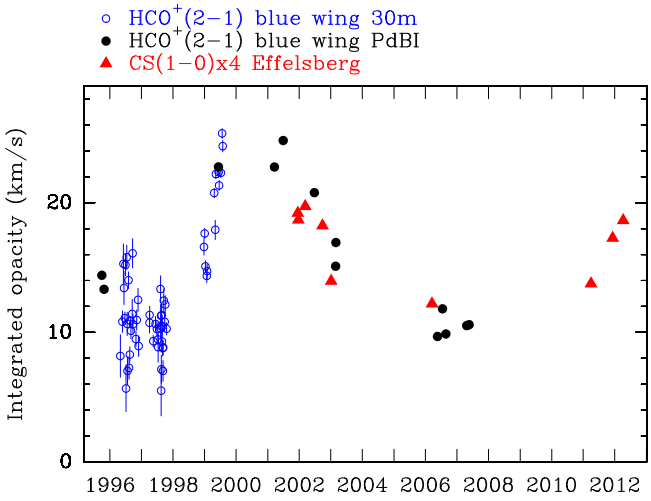

Fig. 4. Integrated opacities for f_c = 0.38 of the blue wing of the HCO^+ J = 2←1 lines (–37.6 km s^{-1} < $V_{\rm LSR}$ < –2.6 km s^{-1}; $V_{\rm LSR} = V_{\rm HEL}$ + 12.4 km s^{-1}; z = 0.88582). The HCO^+ spectra were taken from IRAM Pico Veleta (30-m) and Plateau de Bure (PdBI) data published by Muller & Guélin (2008). Their calibration uncertainties are 15% and 1%, respectively. For the Effelsberg data, see Sect. 2.

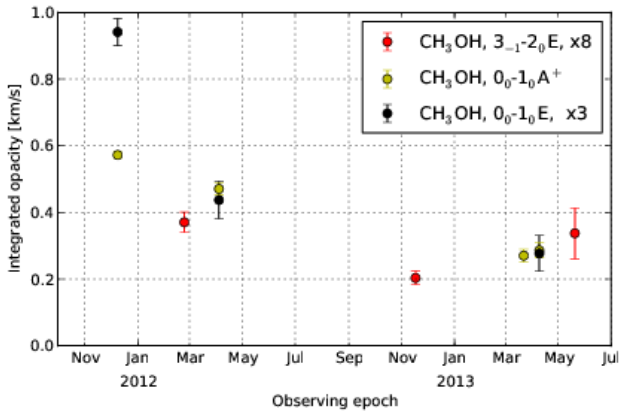

Fig. 5. Integrated opacities of three optically thin methanol (CH_3OH) transitions adopting a continuum source covering factor f_c = 0.38. The data were obtained at Effelsberg (for details, see Bagdonaite et al. 2013a,b) and are shown to demonstrate the decline in opacities during 2012/3 in a qualitative way. Note that the 1_0←0_0 E and the 2_0←3_{-1} E opacities were multiplied by (arbitrary) factors of 3 and 8, to bring values of all lines to roughly the same y-axis scale. Calibration uncertainties are of order 10% or smaller.

H_2CO

Formaldehyde can be efficiently produced on the surface of icy grains through hydrogenation of CO (e.g., Aladro et al. 2011). Interpolating the continuum flux density of the background source of PKS 1830–211 at 7.7 GHz from data at 5 GHz and 8.4 GHz (Subrahmanyan et al. 1990; Nair et al. 1993; Xu et al. 1995; van Ommen et al. 1995; Mattox et al. 1997;, Lovell et al. 1998) yields 7.1 Jy for the fre-

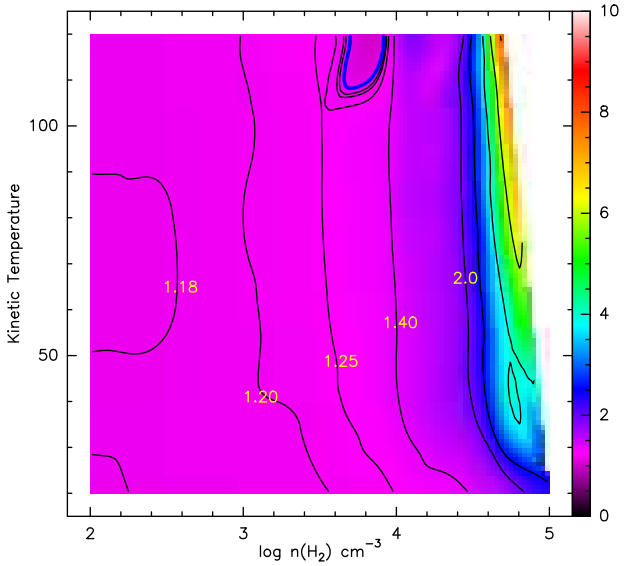

Fig. 6. The 2_{02}←1_{11} to 1_{11}←0_{00} opacity ratio of cyclic para-cyclopropenylidene (para c-C_3H_2) under optically thin conditions as a function of density and temperature. Depending on the continnum source covering factors used (see subsection c-C_3H_2 in Sect. 4.2), we obtain ratios of 0.87±0.19 and 1.14±0.25. Both values are below the modelled ones, but accounting for the errors, they are not inconsistent with the standard values of $T_{\rm kin}$ = 50–80 K and $n(H_2)$ = 1000–2000 cm^{-3} (Henkel et al. 2008, 2009; Muller et al. 2011, 2013).

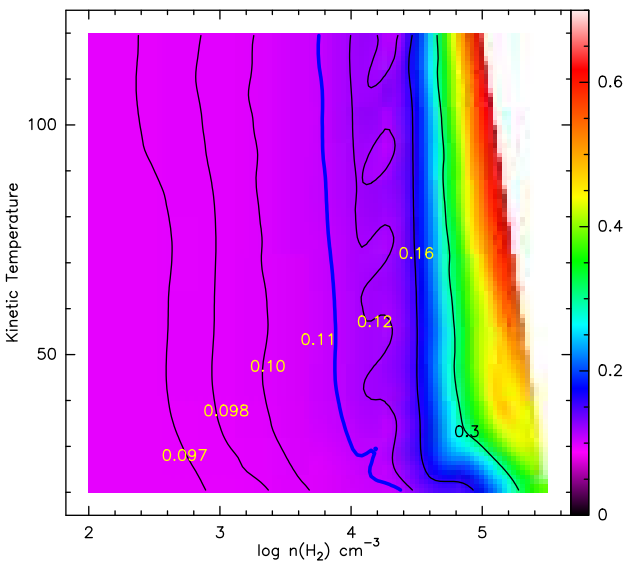

Fig. 7. The 3_{12}←3_{03} to 2_{12}←1_{01} opacity ratio of cyclic ortho-cyclopropenylidene (ortho c-C_3H_2) under optically thin conditions as a function of density and kinetic temperature. The blue almost vertical line represents the measured value (0.110±0.015; Sect. 4.2). When accounting for the error, this is not inconsistent with the standard values given in the caption to Fig. 6.

quency of the (2_{11} ← 2_{12}) line observed by Menten et al. (1999). Their absorption feature of 0.073 Jy therefore absorbs at its peak ∼1% of the total continuum flux density of PKS 1830–211. From that, the derived τ becomes 0.026 for a fixed f_c = 0.38. The observed τ ratio of the 3_{12} ← 3_{13} to 2_{11} ← 2_{12} lines is then of order unity while the model calculation for the temperature and density used above yields a ratio of 0.14 (Fig. 9). To fit a ratio of 1 to 2, any temperature between 10 and 150 K would require densities $n(H_2) \gtrsim 5{\times}10^5$ cm^{-3}. However, accounting for the fact that the 2_{11} ← 2_{12} line is measured at low frequency ($\nu_{\rm observed}$ ∼ 7.68 GHz) and that therefore the source covering factor may be smaller, we obtain with the frequency dependent source covering factor (see Sect. 4.1) originally proposed by Henkel et al. (2009) f_c = 0.108 and an optical depth of 0.10. The resulting 3_{12} ← 3_{13} to 2_{11} ← 2_{12} ratio of optical depths would then become ∼0.54±0.17, still favoring a density of order 10^5 cm^{-3} (see Fig. 9), which would be consistent with the average density deduced by Mangum et al. (2013) from the 1_{10}←1_{11} and 2_{11}←2_{12} transitions of H_2CO toward nearby actively star forming galaxies. If we adopt for our line a dip half as deep, the ratio would become ∼0.25–0.3 and would reduce the density by half an order of magnitude, which is still rather large. To bring our so far preferred model (with $T_{\rm kin}$ = 80 K and $n(H_2)$ = 2000 cm^{-3}) into rough accordance with the observations, our 3_{12} ← 3_{13} line should be weaker by a factor of ∼4, which is inconsistent with the data (see Sect. 5 for a discussion of this result, which indicates strong deviations from the "canonical" physical parameters obtained in previous studies).

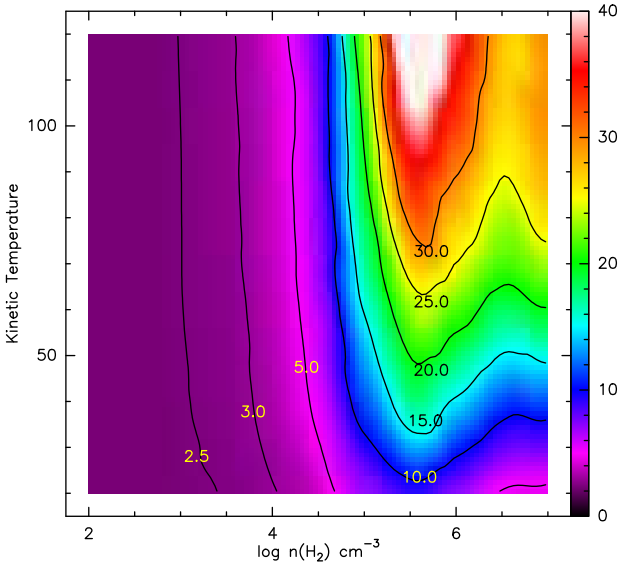

Fig. 8. The 1_0←2_{-1} to 1_0←0_0 opacity ratio of E-type methanol (CH_3OH) under optically thin conditions as a function of density and kinetic temperature. The value of 1.8±0.4 (Sect. 4.2), deduced from measurements, indicates a low density which is, within the error, consistent with the standard parameters given in Fig. 6.

SO

Sulfur monoxide molecules are formed in a high temperature environment by neutral-neutral reactions with high activation energy (e.g., Takano et al. 1995). Both lines used for modelling (see Table 2) are from our observations. The line shapes appear to differ from those of the other transi-

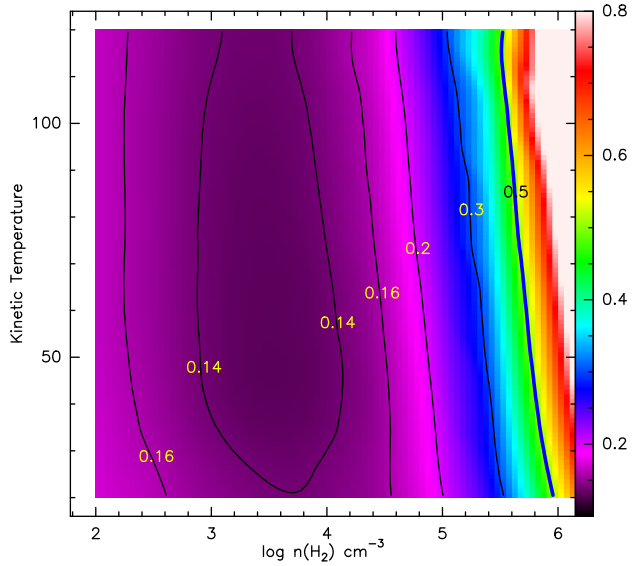

Fig. 9. The 3_{12}←3_{13} to 2_{11}←2_{12} opacity ratio of ortho-formaldehyde (o-H_2CO) under optically thin conditions as a function of density and kinetic temperature. The blue thick almost vertical line on the right hand side denotes a line ratio of 0.5 (Sect. 4.2; the ratio obtained with frequency dependent continuum source covering factors is 0.54±0.17). Here the density is not consistent with the standard value given in the caption to Fig. 6.

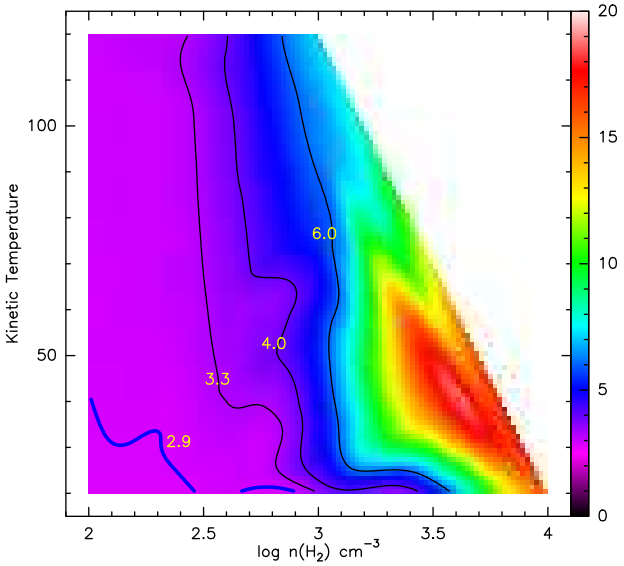

Fig. 10. The 2_1←1_0 to 1_0←0_1 opacity ratio of sulfur monoxide (SO) under optically thin conditions as a function of density and kinetic temperature. With ratios of 2.0±0.5 or 2.9±0.6, depending on the adopted continuum cource covering factors, the density is below that of the standard value given in Fig. 6. The thick blue line in the lower left corner denotes a ratio of 2.9.

tions displayed in Fig. 1 showing a redshifted line wing. In case of the $2_1 \leftarrow 1_0$ line, a small part of the redshifted absorption might be due to the $3_{03} \leftarrow 2_{02}$ line of cyanic acid (HOCN), which is displaced by 28.0 km s^{-1} and contains hyperfine structure components scattered over 10.7 km s^{-1}. However, this molecule is rarely detected in the interstellar medium (see Brünkens et al. 2010) and the profile of the other SO transition (the $1_0 \rightarrow 0_1$ line) looks similar. Following Table 2, our measured 2_1←1_0/1_0←0_1 peak opacity ratios are 2.0±0.5 (f_c = 0.227 and 0.156) and 2.9±0.6 (f_c = 0.38). With T_{kin} = 80 K, gas densities become very low (a few 100 cm^{-3} or less) to fit the observed line ratio (see Fig. 10), which is much lower than that suggested by, e.g., Henkel et al. (2009). On the other hand, choosing a value near their $n(H_2)$ = 2000 cm^{-3}, the modelled gas temperature drops to $\lesssim$20 K, in strong contradiction to NH_3 and CH_3CN data (Henkel et al. 2008; Muller et al. 2011).

The two modelled cases with different source covering factors are in accordance with the upper limit of τ determined from the non-detection of the $4_3 \leftarrow 3_3$ line. The only possible assumption to reconcile the result related to the narrow component with those from NH_3, HC_3N, and CH_3CN (Henkel et al. 2008, 2009; Muller et al. 2011, 2013), and our results from C_3H_2 and CH_3OH is that the absorbing molecular gas shows strong gradients at least in density and possibly also in T_{kin} (see also Sect. 5).

4.3. Column densities and abundances

Our modelled molecular column densities are presented in Table 4 as well as abundance ratios relative to CO and H_2. Our abundance ratios are generated using $N_{CO} = 3 \times 10^{18}$ cm^{-2} (Gerin et al. 1997) and $N_{H_2} = 3 \times 10^{22}$ cm^{-2} (Gerin et al. 1997, Wiklind & Combes 1996a). This is also discussed by Muller et al. (2011). Depending on the background source covering factor (f_c = 0.38 or frequency dependent; see Table 2) there is in most cases an uncertainty by a factor of almost two in the column densities. Here we refer to average values between these two extremes, providing accordingly ±40% errors.

To compare our results with those of Menten et al. (1999) obtained at the VLA, we take molecular column densities and their ratios to CO directly from their Table 1, while we derive their ratio to H_2 using the H_2 column density mentioned above. For comparison with results by Muller et al. (2011), we use their N_{mol} from their Table 3, and N_{CO} (as mentioned above) from Wiklind & Combes (1996a) and Gerin et al. (1997). Note that our chosen N_{H_2} value is 50% larger than that adopted by Muller et al. (2011) in their Table 8.

c – C_3H_2: Our total column density is about an order of magnitude higher than that of Menten et al. (1999), but is in good agreement with that of Muller et al. (2011). These factors also apply to the ratios relative to CO and H_2.

CH_3OH: Our column density and relative abundance are in good accordance with Muller et al. (2011) and also with Bagdonaite et al. (2013a,b).

H_2CO: Our values agree well with those of Menten et al. (1999), while those of Muller et al. (2011) are almost an order of magnitude smaller.

SO: Our column density is in accordance with the value given by Muller et al. (2011). Their abundance relative to H_2 is almost identical to our result. For all temperatures between 20 K and 80 K, resulting column densities are similar within a factor of <2.

SiS, HNCO: Our non-detections yield upper limits to the molecule's abundances relative to H_2. The one for

Table 4. Kinetic temperatures, densities, column densities N, and fractional abundances $N/N_{\rm CO}$ and $N/N_{\rm H_2}$

Molecule	Temperature (K)	Gas density ($\rm cm^{-3}$)	N ($10^{12}\,\rm cm^{-2}$)	$N_{\rm Lit.}$	$N/N_{\rm CO}$ (10^{-6})	$N/N_{\rm CO}$(Lit.) (10^{-6})	$N/N_{\rm H_2}$ (10^{-9})	$N/N_{\rm H_2}$(Lit.) (10^{-9})
o+p c-C_3H_2	80	2000	65 (±40%)	7 (Me) 53 (Mu)	22	2 (Me) 17 (Mu)	2.2	0.23 (Me) 1.8 (Mu)
CH_3OH	80	2000	140 (±40%)	170 (Mu)	45	57 (Mu)	4.5	5.6 (Mu)
o-H_2CO	10–150	$> 5 \times 10^4$	400 (±40%)	380 (Me) 60 (Mu)	130	130 (Me) 20 (Mu)	13.0	13 (Me) 2 (Mu)
SO	20–80	400–2000	35 (±50%)	26 (Mu)	12	9 (Mu)	1.2	0.9 (Mu)
SiS	80	2000	<5.		<2.5		<0.2	
HNCO	80	2000	<8.6	6.2(Mu)	<4	2.1 (Mu)	<0.3	0.2 (Mu)

Col. (1): Molecular species; Col. (2): Adopted kinetic temperature; Col. (3): Adopted gas density; Col. (4): Our column densities; Col. (5): Column densities derived from data of Menten et al. (1999) (Me) and Muller et al. (2011) (Mu) in the way described in Sect. 4.3; Cols. (6) and (7): same as Cols. (4) and (5), but relative to the adopted CO column density, $N_{\rm CO} = 3 \times 10^{18}\,\rm cm^{-3}$ (Sect. 4.3); Cols. (8) and (9): same as Cols. (4) and (5), but relative to the adopted H_2 column density, $N_{\rm H_2} = 3 \times 10^{22}\,\rm cm^{-3}$ (see Sect. 4.3).

HNCO is in accordance with the value derived by Muller et al. (2011) from a detected $J = 3 \leftarrow 2$ line.

4.4. Excitation temperatures

Some of the molecular lines we have measured exhibit excitation temperatures, which are quite far from the expected $T_{\rm CMB}$ value, $T_{\rm CMB} = 2.73\,\rm K \times (1+z) = 5.14\,K$ (Muller et al. 2013; Sato et al. 2013). The $J_{\rm KaKc} = 3_{12} \leftarrow 3_{13}$ line of H_2CO, for example, is collisionally cooled (e.g., Evans et al. 1975; Zeiger & Darling 2010; Darling & Zeiger 2012) and may show, in spite of the uncertainties w.r.t. density (Sect. 4.2), excitation temperatures well below 5.14 K. The second example is the SO $1_0 \leftarrow 0_1$ transition. Applying our LVG code, it exhibits for the standard parameters $T_{\rm kin} = 80\,\rm K$ and $n(H_2) = 2000\,\rm cm^{-3}$ excitation temperatures of several 10 K degrees or even inversion in case of $T_{\rm CMB} < 4.0\,\rm K$. In case of lower $T_{\rm kin}$ and density, however, e.g., for 40 K and $1000\,\rm cm^{-3}$ (see Sect. 4.2), the excitation temperature becomes "well behaved" for $3\,\rm K < T_{CMB} < 7\,K$, only surpassing the $T_{\rm CMB}$ value by 2.0–2.5 K. On the other hand, the LVG calculations indicate that the excitation temperatures of para and ortho c-C_3H_2, CH_3OH, and the $2_1 \leftarrow 1_0$ transition of SO are normal in the sense that they are slightly higher than the $T_{\rm CMB}$ value and rise with increasing density (cf. Fig. 3 of Muller et al. 2013). For $n(H_2) = 2000\,\rm cm^{-3}$, $T_{\rm kin} = 80\,\rm K$, and $3\,\rm K < T_{CMB} < 7\,K$, the C_3H_2 and $1_0 \leftarrow 0_0$ CH_3OH (E) excitation temperatures are within 5% and slightly above the chosen cosmic microwave value. This emphasizes that these lines are suitable tools to constrain $T_{\rm CMB}$ at redshift $z \sim 0.89$ and confirms the assumption of $T_{\rm ex} \ll T_{\rm C}$ ($T_{\rm C} \gtrsim 10^7\,\rm K$; e.g., Jin et al. 2003), used to calculate optical depths (see Sect. 3).

5. Discussion

The frequencies of our observations range from 15 to 35 GHz, those of Muller et al. (2011) and Menten et al. (1999) from 30 to 50 GHz with the exception of the H_2CO ($2_{11} \leftarrow 2_{12}$) line at 7.7 GHz. The size of the SW spot of the background continuum source lensed by the foreground galaxy is reported to decrease with frequency (e.g. Carilli et al. 1998, Garrett et al. 1998, Jin et al. 2003), but the sizes given there for a specific frequency do not agree with each other. Nevertheless, at the highest observing frequency of 45 GHz discussed in our analysis, this size must be larger than 0.2 milliarcsec, which corresponds to ∼2 pc linear extent.

Within the limitations by noise, all our spectra as well as the used spectra of the referenced literature show compatible center velocities (see, e.g., also Henkel et al. 2008 and Muller et al. 2014b). Therefore, we assume that they all originate from the same cloud complex. In particular, we also find that the line widths do not depend on the frequency of the studied feature (see also Henkel et al. 2008, 2009 for complementary lines). Observing molecular cloud material of $\gtrsim$2 pc linear extent along a line-of-sight with a likely larger depth, a line width of ∼10–20 $\rm km\,s^{-1}$ (neglecting the $V \sim 175\,\rm km\,s^{-1}$ component reported by Muller et al. 2014b) consisting of several kinematic subcomponents (e.g., Muller et al. 2008; Murphy et al. 2008; Henkel et al. 2009) could be readily expected by a combination of "normal" clouds (e.g., Larson 1981).

From their ammonia multi-line analysis, Henkel et al. (2008) conclude that 80% to 90% of the ammonia gas has a kinetic temperature of about 80 K. But since rotational temperatures of the ammonia gas vary from 35 K to up to 600 K, they also state that the gas may show large temperature gradients. Our line analysis above indicates for the first time strong density gradients (for variations by a factor of two, see also Muller et al. 2013). As Henkel et al. (2008) point out, kinetic temperatures are far too large for a dark-cloud-scenario. The different temperature/density parameters obtained indicate instead a combination of outer cloud layers and/or intercloud regions as well as denser cloud cores.

This "mixture" of physical properties is also supported by a comparison of molecular abundances with those of different types of Galactic objects. For the following comparison of our abundance values to those of sources with

different character, we use values of different cloud types contained in Table 8 of Muller et al. (2011) for our observed molecules. There is overlap with Table 1 of Menten et al. (1999) only for the source TMC 1 and for the molecules C_3H_2 and H_2CO; these values agree with each other.

Our C_3H_2 abundance agrees with those of low density molecular clouds and lies between those of the starburst galaxies NGC 253 and NGC 4945. Fractional abundances for translucent clouds as well as TMC 1 are much higher. For CH_3OH, our abundance is similar to that of NGC 4945, in between those of translucent clouds and TMC 1, whereas that of NGC 253 is a moderate factor of 2 higher. The H_2CO abundance is an order of magnitude higher than in the starburst galaxies, half an order of magnitude higher than in diffuse and translucent clouds, and is within the uncertainties (factors of two) compatible with that of TMC 1. Our SO abundance agrees with those of both starburst galaxies, whereas those of translucent clouds and the TMC 1 are higher. In contrast, our upper limit as well as the value for HNCO agrees with that of the TMC 1 and Sgr B2; here, abundances of translucent clouds and the starburst galaxies are higher.

All this increasingly indicates that former interpretations attempting to attribute observed molecular abundances to one distinct cloud type do not lead to a realistic scenario of the interstellar matter we observe toward south-western molecular hotspot of PKS 1830–211. We possibly observe a cloud complex which is with respect to spatial fine structure similar to cloud complexes in our own Galaxy. With the dust-to-gas ratio in PKS 1830–211 being consistent with the Galactic value (Dai et al. 2006; Aller et al. 2012), we apparently observe a combination of different conditions in different cloud types which should not be surprising for a region encompassing several pc in the plane of the sky and presumably an even larger linear scale along the line-of-sight.

Henkel et al. (2008), not yet being aware of the $V \sim 175\,\mathrm{km\,s^{-1}}$ feature reported by Muller et al. (2014b), discuss the scenario that the south-western absorbing cloud toward PKS 1830–211 may be similar to the gas seen toward Sgr B2 in our Galaxy. What they miss is a similar molecular condensation located at several kpc from the center as it is seen toward PKS 1830–211. Line widths of various species observed at various linear scales in Sgr B2 (0.4 – 2.5 pc) are of order $20\,\mathrm{km\,s^{-1}}$ (Rohlfs et al. 2010, Comito et al. 2003). Apparently at ∼7 Gyr in the past, also a cloud complex at 2–3 kpc galactocentric distance can show this fingerprint.

6. Conclusions

From our excitation analysis of molecular line spectra of various species applying a Large Velocity Gradient radiative transfer model, we draw the following conclusions:

- For the c-C_3H_2 and CH_3OH molecules, the data are compatible with $T_{\rm kin} = 80$ K and $n(H_2) = 2000\,\mathrm{cm^{-3}}$, in accordance with previously reported results, indicating gas of low density.
- While our observed H_2CO K-doublet line is noisier than that of Menten et al. (1999), the resulting τ values of both lines are very similar, yielding volume densities $n(H_2) \gtrsim 5 \times 10^5\,\mathrm{cm^{-3}}$ for all kinetic temperatures between 10 K and 80 K. An absorption dip half as deep as that derived from our data, which still might be adopted as an extreme, would reduce the density to $n(H_2) \sim 5 \times 10^4\,\mathrm{cm^{-3}}$, which still is more than an order of magnitude higher than the one derived by Henkel et al. (2009) on the basis of an HC_3N multiline analysis.
- For the SO molecule, if we assume $T_{\rm kin} = 80$K, the volume gas density becomes extremely low ($n(H_2) \lesssim 500\,\mathrm{cm^{-3}}$). If we raise the density to $2000\,\mathrm{cm^{-3}}$, the kinetic temperature drops to 20 K. Both models as well as those in between these two extremes result in about the same column density (see Table 4.2).
- Our resulting densities and relative molecular abundances are in fair if not good agreement with those found in the local universe. This is in accordance with the statement of Aller et al. (2012) that "there is also evidence that the dust-to-gas ratio in this system is consistent with the Galactic value".
- For the south-western hotspot of PKS 1380–211, there is a trend of rising integrated opacities during the late nineties, with peaks near 2001, followed by a minimum around 2006. In recent years, opacities were rising again, reaching a maximum in 2011/2012. In the long term we may test for periodicities, possibly probing a putative precessing jet in the background blazar. In this context, long term monitoring of both the south-western and north-eastern velocity components would be instructive.
- Molecules are known to have different abundances in different types of clouds (e.g., Menten et al. 1999; Muller et al. 2011). Together with the fact that the lines analyzed here reflect different physical conditions, we conclude that, within the observed region of a few pc in size along the plane of the sky and likely a larger depth along the line-of-sight, there are strong gradients in density and likely also in temperature. To summarize, we see a combination of conditions typical for different types of molecular gas.

Acknowledgements. We wish to thank an anonymous referee for useful comments. We used NASA's Astrophysical Data System (ADS), the Cologne Database for Molecular Spectroscopy (CDMS; see Müller et al. 2001, 2005), the JPL Catalog (http://spec.jpl.nasa.gov/ftp/pub/catalog/catform.html), and the line lists of Lovas (1992) and Coudert & Roueff (2006).

References

Aladro, R., Martin-Pintado, J., Martin, S., Mauersberger, R., & Bayet, E. 2011, A&A, 525, A89
Aller, M. C., Kulkarni, V. P., York, D. G., et al. 2012, ApJ, 748, 19
Bagdonaite, J., Jansen, P., Henkel, C., et al. 2013a, Sci, 339, 46
Bagdonaite, J., Daprà, M., Jansen, P. et al. 2013b, Phys. Rev. Let., 111, 231101
Brünkens, S., Belloche, A., Martín, S., Verheyen, L., Menten, K.M. 2010, A&A, 516, 109
Carilli, C. L., Menten, K. M., Reid, M. J., Rupen, M., & Claussen, M. 1998, in *Radio Emission from Galactic and Extragalactiv Compact Sources*, eds. A. Zensus et al., ASP Conference Series, 144, 317
Comito, C., Schilke, P., Gerin, M., et al. 2003, A&A 402, 635
Coudert, L. H., & Roueff, E. 2006, A&A, 449, 855
Courbin, F., Meylan, G., Kneib, J.-P., & Lidman, C. 2002, ApJ, 575, 95
Dai, X., Chartas, C. S., & Mathur, S. 2006, ApJ, 637, 53
Darling, J., Zeiger, B. 2012, ApJ, 740, L33
De Rosa, A., Piro, L., Tramacere, A., et al. 2005, A&A, 438, 121
Evans, N. J., Morris, G., Sato, T, & Zuckerman, B. 1975, ApJ, 196, 433
Garrett, M. A., Leppänen, K., Porcas, R. W, et al. 1998, in *Radio Emission from Galactic and Extragalactic Compact Sources*. eds/ A. Zensus et al., ASP Conf. Ser., 144, 313

Gerin, M., Phillips, T. G., Benford, D. J., et al. 1997, ApJ, 488, L31
Henkel, C., Braatz, J. A., Menten, K. M., & Ott, J. 2008, A&A, 485, 451
Henkel, C., Menten, K.M., Murphy, M.T., et al. 2009, A&A, 500, 725
Jauncey, D.L., Reynolds, J.E., Tzioumis, A.K., et al. 1991, Nature 352, 132
Jin, C., Garrett, M. A., Nair, S., et al. 2003, MNRAS, 340, 1309
Kanekar, N., Carilli, C. L., Langston, G. I., et al. 2005, Phy. Rev. Let. 95, 261301
Leurini, S., Schilke, P., Menten, K. M., et al. 2004, A&A, 422. 573
Lidman, C., Courbin, F., Meylan, G., Broadhurst, T., Frye, B., Welch, W.J.W. 1999, ApJ, 514, L57
Liszt, H.S., Pety, J., Lucas, R. 2008, A&A, 486, 493
Lovell, J.E.J., Jauncey, D.L., & Reynolds, J.E., 1998, ApJ, 508, L51
Larson, R. B. 1981, MNRAS, 194, 809
Lovas, F. J. 1992, J. Phys. Chem. Ref. Data, 21, 181
Madden, S. C., Irvine, W. M., Matthews, H. E., Friberg, P., & Swade, D. A. 1989, AJ, 97, 1403
Mangum, J., Darling, J., Henkel, C., & Menten, K. M. 2013, ApJ, 766, 108
Martí-Vidal, I., Muller, S., Combes, F., et al. 2013, A&A, 558, A123
Mattox, J.R., Schachter, J., Molnar, L., Hartman, R.C., & Patnaik, A.R. 1997, ApJ, 481, 95
Menten, K. M., Carilli, C., & Reid, M. J. 1999, in *Highly Redshifted Radio Lines*, ed. C. Carilli et al., ASP Conference Series, 156, 218
Menten, K.M., Güsten, R., Leurini, S., et al. 2008, A&A 492, 725
Müller, H. S. P, Thorwirth, S., Roth, D.A., & Winnewisser, G. 2001, A&A 370, L49
Müller, H. S. P, Schlöder, F., Stutzki, J., & Winnewisser, G. 2005, J. Mol. St. 742, 215
Muller, S., Guélin, M., Dumke, M., Lucas, R., & Combes, F. 2006, A&A, 458, 417
Muller, S. & Guélin, M. 2008, A&A, 491, 739
Muller, S., Beelen, A., Guélin, M., et al. 2011, A&A, 535, A 103a
Muller, S., Beelen, A., Black, J.H., et al. 2013, A&A, 551, A109
Muller, S., Black, J. H., Guélin, M., et al. 2014a, A&A, 566, L6
Muller, S., Combes, F., Guélin, M., et al. 2014b, A&A, 566, A112
Murphy, M. T., Flambaum, V. V., Muller, S., & Henkel, C. 2008, Sci, 320, 1611
Nair, S., Narasimha, D., & Rao, A. P. 1993, ApJ, 407, 46
Nair, S., Jin, C., & Garrett, M. A. 2005, MNRAS, 362, 1157
Planck Collaboration, Ade, P. A. R., Aghanim, N., et al. 2014, A&A, 571, A16
Rolffs, R., Schilke, P., Comito, C. et al. 2010, A&A, 521, L46
Sato, M., Reid, M. J., Menten, K. M., & Carilli, C. L. 2013, ApJ, 764, 132
Subrahmanyan, R., Narashima, D., Rao, A.P., & Swarup, G. 1990, MNRAS, 246, 263
Takano, S., Nakai, N., & Kawaguchi, K. 1995, PASJ, 47, 801
Thaddeus, P., Vrtilek, & J. M., Gottlieb, C. A. 1985, ApJ, 299, L63
van Ommen, T.D., Jones, D.L., Preston, R.A., & Jauncey, D.L. 1995, ApJ, 444, 561
Wiklind, T., & Combes, F. 1994, A&A, 286, L9
Wiklind, T., & Combes, F. 1995, A&A, 299, 382
Wiklind, T., & Combes, F. 1996a, Nature, 379, 139
Wiklind, T., & Combes, F. 1996b, A&A, 315, 86
Wiklind, T., & Combes, F. 1998, ApJ, 500, 129
Winn, J.N., Lovell, J.E.J., Chen, H-W., et al. 2002, ApJ, 564, 143
Xu, W., Readhead, A.C.S., Pearson, T.J., Polatidis, A.G., & Wilkinson, P.N. 2005, ApJS, 99, 297
Zeiger, B. & Darling, J. 2010, ApJ, 709, 386